ACS APPLIED MATERIALS & INTERFACES

Research Article

www.acsami.org

Facilitation of High-Rate NADH Electrocatalysis Using Electrochemically Activated Carbon Materials

Hanzi Li, Rui Li, Robert M. Worden, and Scott Calabrese Barton*

Department of Chemical Engineering and Materials Science, Michigan State University, East Lansing, Michigan 48824, United States

Supporting Information

ABSTRACT: Electrochemical activation of glassy carbon, carbon paper and functionalized carbon nanotubes via high-applied-potential cyclic voltammetry leads to the formation of adsorbed, redox active functional groups and increased active surface area. Electrochemically activated carbon electrodes display enhanced activity toward nicotinamide adenine dinucleotide (NADH) oxidation, and more importantly, dramatically improved adsorption of bioelectrochemically active azine dyes. Adsorption of methylene green on an electroactivated carbon electrode yields a catalyst layer that is 1.8-fold more active toward NADH oxidation than an electrode prepared using electropolymerized methylene green. Stability studies using cyclic voltammetry indicate 70% activity retention after 4000 cycles. This work further facilitates the electrocatalysis of NADH oxidation for bioconversion, biosensor and bioenergy processes.

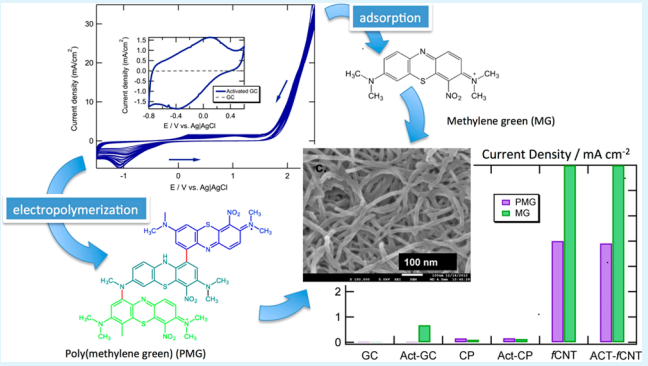

KEYWORDS: *electrochemical activation, carbon nanotube, glassy carbon, NADH electrocatalysis, azine adsorption, activity facilitation*

INTRODUCTION

The effective recycling of nicotinamide adenine dinucleotide ($NADH/NAD^+$) is of great interest, because $NADH/NAD^+$ acts as an essential cofactor in ubiquitous redox enzymes that are widely applicable in biosensor, bioenergy and bioconversion processes. For example, $NADH/NAD^+$ is involved in the naturally occurring enzymatic reactions of glycolysis, Kreb's cycle and oxidative phosphorylation.[1] Biosensors reported for glucose,[2,3] glycerol,[4,5] lactate,[6] isocitrate[7] and alcohol[8−13] are based on NADH monitoring systems with relevant dehydrogenases. Combining cofactor NAD^+ regeneration with enzyme catalyzed reactions allows one to utilize a great number of inexpensive fuels, e.g., methanol[14,15] and ethanol,[16] and develop efficient biofuel cells.[17,18] Applications of NADH-dependent dehydrogenases to produce value-added chemicals have been studied as well, such as production of dihydroxyacetone from glycerol[19−21] and methanol from CO_2.[22]

A key challenge in electrochemically regenerating NAD^+ is the high overpotential required due to slow kinetics on conventional electrodes. Strategies to address this issue include electrode modification by electrocatalysts, such as quinones,[23−26] phenazine and phenoxazine dyes,[27−31] poly(aniline),[32] metal oxides[33,34] and the enzyme diaphorase.[14] Recently, use of different forms of carbon, such as pyrolytic graphite,[35] graphene oxide[36] and especially porous, high surface area materials, such as carbon nanotubes (CNT)[4,9,28,37] and "Bucky" paper,[38] have also been investigated. We previously described a method to facilitate NADH oxidation by electropolymerizing azines on electrodes modified by functionalized carbon nanotubes (fCNT).[28,39] In this work, we describe a novel method to further facilitate NADH electrocatalysis by adsorption of azine electrocatalysts on electroactivated carbon surfaces.

Activation is a well-known approach to increasing carbon electrode reactivity.[40] The key principle of carbon material activation is to modify the carbon surface by increasing surface roughness and introducing carbon−oxygen functionalities.[40−51] For example, Epstein et al. studied voltammetry-activated isotropic pyrolytic graphite and suggested the formation of quinine−hydroquinone groups.[52] Reported carbon activation procedures include laser irradiation,[51,53] high-intensity ultrasonication,[50] heating[48] and UV−ozone treatment.[54] Electrochemical pretreatment, however, is attractive because of its effectiveness in mild operation conditions.[41−47,49]

Glassy carbon (GC) is a widely used conventional electrode material due to its high conductivity, hardness and inertness.[55] Laser et al. proposed the mechanism of carbon−oxygen group formation on the surface of GC: chemical adsorption of oxygen under anodic polarization, followed by oxidation and reduction of existing surface groups and the evolution of oxygen from water.[56] Čenas et al. reported quinoidal structures of oxidatively treated GC and demonstrated its increased catalytic activity for NADH oxidation.[57] Recent reports on electrochemical activation of GC involve cyclic voltammetry-activated GC for

Received: January 19, 2014
Accepted: April 2, 2014
Published: April 2, 2014

   dx.doi.org/10.1021/am500087a | ACS Appl. Mater. Interfaces 2014, 6, 6687−6696

chloranil adsorption,[46] constant potential treated GC for hydroquinone and catechol sensor.[47]

Porous materials such as carbon paper,[58] carbon foam[59] and carbon nanotubes[37,54,60,61] introduce intrinsically high surface area and may also be electrochemically activated.[40,59] Oxidative treatment of carbon nanotubes is a key method for increasing their hydrophilicity.[37,54,60,61] However, the literature shows inconsistency regarding the effect of electrochemical pretreatment on CNT.[62,63] For example, Gong et al. reported that electrochemical activation of vertically aligned CNT at 1.8 V for 3 min in pH 6.5 phosphate buffer electrolyte leads to a reduction of NADH oxidation overpotential by 450 mV.[62] However, a study by Musameh et al. shows no change of NADH electrocatalysis after electrochemically oxidizing CNT at 1.75 V for 3 min in pH 7.4 phosphate buffer.[63]

This work utilizes high-applied-potential cyclic voltammetry to activate glassy carbon (GC), carbon paper (CP) and functionalized carbon nanotubes (*f*CNT). Electrochemical activation leads to the formation of redox active groups on the electrode surface and increased active surface area. These activated carbon materials allow subsequent adsorption of the electrocatalyst methylene green (MG), forming a novel NADH-oxidizing interface. The activity of MG-*f*CNT toward NADH oxidation is higher than that of our previously reported poly(azine)-*f*CNT electrodes,[28] demonstrating an improved facilitation of NADH electrocatalysis.

EXPERIMENTAL SECTION

Materials. Glassy carbon rotating disk electrodes (GC) with diameter of 3 mm were made from type 2 GC rods (Alfa Aesar, Ward Hill, MA). Before use, these were sanded with 400, 800, 2400 and 4000 grit ultrafine sandpapers (Buehler, IL), polished to a mirror finish with 0.05 μm alumina slurry and rinsed with distilled water in an ultrasonic bath for 10 min to remove any residual alumina. Multiwall carbon nanotubes, functionalized by carboxylation (*f*CNT, 9.5 nm diameter, 1.5 μm length and >95% purity) were purchased from Nanocyl (Sambreville, Belgium, catalog number: NC3101). Carbon paper was purchased from Electrochem, Inc, (Woburn, MA, catalog number: EC TP1 030). NADH, methylene green (MG), sodium tetraborate and sodium nitrate were obtained from Sigma-Aldrich (St. Louis, MO). *N*,*N*-dimethylformamide (DMF) was purchased from Fisher BioReagents (Hampton, NH). Sodium phosphate monobasic and sodium phosphate diabasic were purchased from J.T. Baker (Phillipsburg, NJ). Argon gas was purchased from Airgas (Lansing, MI). Unless otherwise stated, all materials were used as received.

CNT Coating on GC and CP. As previously reported,[28,64] CNT were dispersed in DMF solvent to create 1 mg mL^{-1} ink under ultrasonication. CNT-coated GC electrodes (CNT-GC) were fabricated by drop-casting 5 μL of CNT ink on the GC surface and vacuum drying. For the purposes of elemental analysis, CNT-coated CP was prepared by air-brushing and dried in vacuum.

Electrochemical Activation of Carbon Electrode. GC and CP were activated by cyclic voltammetry (CV) with a scan rate of 100 mV s^{-1} between −1.5 V and +2.5 V vs Ag|AgCl (4 M KCl) in 100 mM, pH 7.45 phosphate buffer. Platinum wire was used as counter electrode. Twenty cycles were conducted at 30 °C. *f*CNT were activated electrochemically using CV for only two cycles; further cycling would lead to detachment of the *f*CNT from the glassy carbon substrate.

Deposition of Azines. Two approaches were used for azine deposition: adsorption and electropolymerization. For adsorption, the activated electrodes were soaked in 1 mM MG solution (100 mM pH 7.45 phosphate buffer, 30 °C) for 1 h. For electropolymerization, CV was performed in MG monomer solution at 50 mV s^{-1} between −0.5 and +1.5 V vs Ag|AgCl for 20 cycles in 10 mM, pH 9.1 borate buffer with 100 mM $NaNO_3$.[65]

Electrochemical Characterization. All electrochemical characterizations were obtained using a VSP potentiostat (Bio-Logic VSP, Knoxville, TN). An Ag|AgCl (4 M KCl) reference electrode was employed with a platinum wire as the counter electrode. The supporting electrolyte used was 100 mM phosphate buffer, pH 7.45, 30 °C, with argon purged to exclude oxygen.

Capacitance was measured by CV in the range of 0.3 to 0.4 V vs Ag|AgCl with scan rates varying from 30 to 150 mV s^{-1}. Plotting the current against scan rate, the slope was recorded as the capacitance. Characterization of redox peaks was performed via CV with scan rate 50 mV s^{-1}. NADH oxidation activity was characterized at 900 rpm by chronoamperometry using independent step changes in polarization and NADH concentration. During polarization studies, NADH concentration was fixed at 1 mM, and steady-state current density at each working potential was recorded. In NADH concentration studies, the working electrode potential was fixed at 50 mV vs Ag|AgCl, and steady-state current density at each NADH concentration was recorded.

Morphology Characterization and Elemental Analysis. As described previously,[28] scanning electron microscopy (SEM, JEOL JSM-7500F, 5.0 kV, 4.5 mm) was used to characterize the morphology of *f*CNT and MG-*f*CNT on the carbon support. Os coating (Neo Osmium coater, Meiwafosis Co., LTD., Tokyo, Japan) was used to obtain clear SEM images.[66] For a 5 s deposition time, an Os layer of 2.5 nm thickness is reported by the manufacturer. Energy-dispersive X-ray spectroscopy (EDS) was applied for elemental quantification, using non-Os coated samples.

RESULTS AND DISCUSSION

Glassy carbon RDEs, CP and *f*CNT were electrochemically activated by CV. MG was then deposited on pretreated carbon electrodes, and these electrodes were further characterized for activity toward NADH oxidation.

Electrochemical Activation. Activation of the GC electrode was achieved by CV over −1.5 to +2.5 V in phosphate buffer, the voltammograms of which are shown in Figure 1. In the 1.5 to 2.5 V range, the evolution of oxygen from water contributes to a large observed oxidation current. Under such anodic polarization, oxygen chemisorbs on the GC surface, presumably at defects in the basal plane sites, according to[56,67,68]

$$C + H_2O \rightarrow C(O) + 2H^+ + 2e^- \quad (1)$$

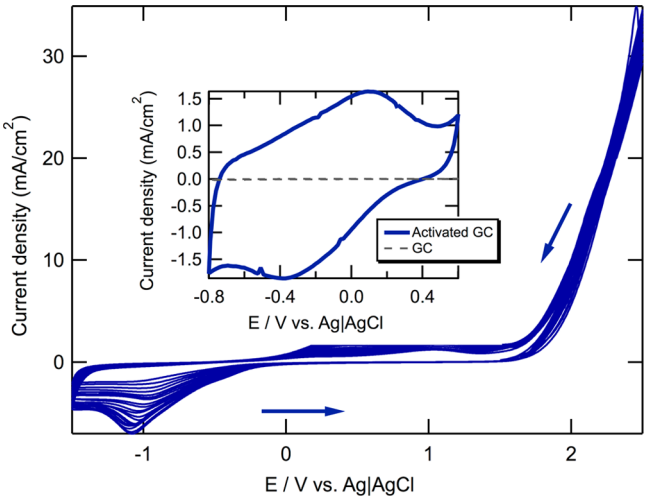

Figure 1. Electrochemical activation of glassy carbon. Cyclic voltammetry was performed on glassy carbon rotation disk electrode, 20 cycles, 100 mV s^{-1}, 0.1 M phosphate buffer, pH 7.45, 30 °C. Inset: cyclic voltammograms of glassy carbon electrode before and after activation in 0.1 M phosphate buffer pH 7.45, 30 °C.

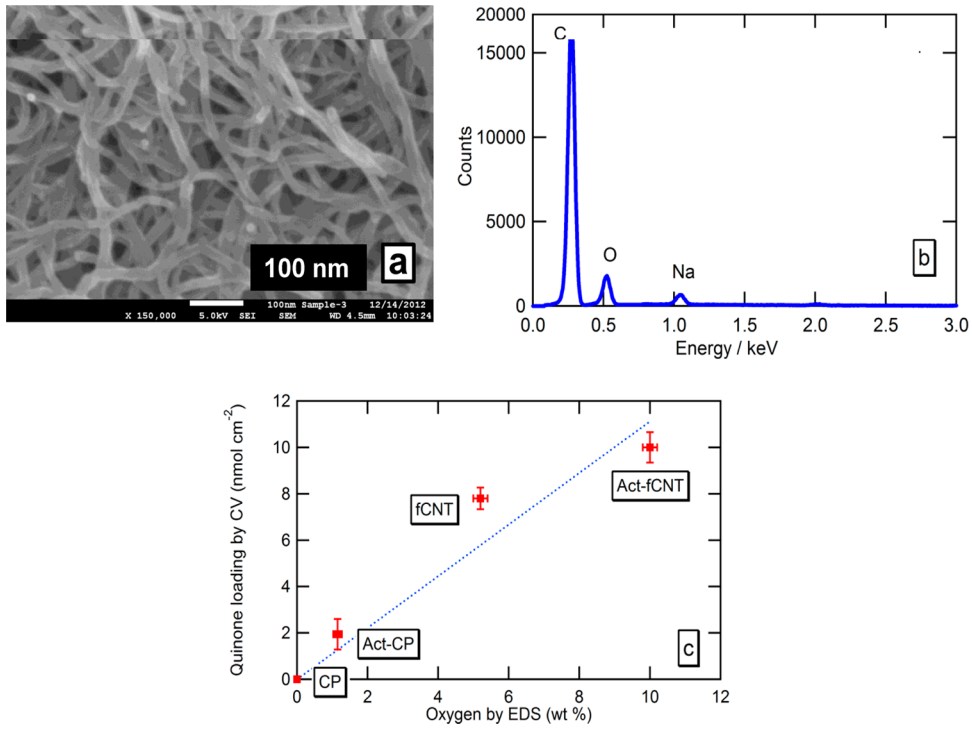

Figure 2. (a) SEM image of Act-*f*CNT; (b) example of energy dispersive X-ray spectroscopy (EDS) spectra on Act-*f*CNT; (c) quantitative properties of electrochemically activated carbon materials. Quinone loading was calculated by integration of cyclic voltammetric (CV) redox peaks in 0.1 M phosphate buffer pH 7.45, 30 °C, assuming a two-electron redox reaction; oxygen mass content was obtained from EDS.

where C(O) represents the possible carbon−oxygen functionalities on electrode surface, such as carboxyl, phenol, carbonyl and quinone.[69]

After the carbon surface carbon is oxidized, electrolytes may penetrate into interlayer spaces, form graphite-oxide layers, and thereby increase the interlayer distance and active surface area.[68,70] Moreover, at such a high polarization potential, aromatic rings can be oxidatively broken and oxidized to CO or CO_2. This process can facilitate the electrochemical activation and porous structure formation in GC.[68]

At low potential (<0 V, especially around −1 V), the cathodic current in Figure 1 is attributable to water reduction. This region is not necessary for electrochemical activation, and it is possible to bypass this cathodic polarization region altogether. Further analysis of the impact of activation conditions is ongoing.

Electrochemically Activated Carbon Electrodes. CV characterization of the electrochemically activated GC electrode (Act-GC) is displayed in the inset of Figure 1. We observe a significant increase of capacitive current as well as an obvious redox peak with a mid-potential around −0.15 V vs AglAgCl. This mid-potential is comparable to the reported redox potentials of quinones,[71] indicating the existence of quinine/hydroquinone couple according to

$$Q + 2H^+ + 2e^- \rightleftarrows QH_2 \quad (2)$$

The existence of redox active quinine/hydroquinone couples has been suggested by Epstein et al.[52] and Čėnas et al.[57] to account for the observed redox response. Other functional groups, such as phenol and carbonyl, have a higher capacitance than bare GC and can lead to an increase in observed double-layer capacitance.[68,69]

For simplicity, we refer here to all redox active groups produced by activation as "quinones". Assuming a two-electron redox reaction (eq 1), quinone loading was determined coulometrically to be 29 ± 5 nmol cm^{-2} for electroactivated GC. A broad redox peak was also observed for electroactivated carbon paper (CP), prefunctionalized CNT (*f*CNT) and further electrochemically activated *f*CNT (Act-*f*CNT, CVs not shown). Quinone loadings for all of these materials were calculated from CV.

The morphology of Act-*f*CNT characterized by SEM is displayed in Figure 2a. A homogeneous porous structure with 50 to 200 nm pores was found, which is very similar to *f*CNT, indicating that electrochemically activation does not change the porous structure of *f*CNT. For all CP samples, with and without *f*CNT, oxygen content was obtained by Energy dispersive X-ray spectroscopy (EDS, shown in Figure 2b). The results were correlated with coulometric quinone loading in Figure 2c, where a linear correlation was found. This reinforces the attribution of the broad voltammetric peak to oxygen-bearing quinoidal species.

Capacitance data are displayed in Figure 3 for a range of materials. Act-GC possesses capacitance as high as (2.4 ± 1.0) ×10^3 μF cm^{-2}, 200-fold above untreated GC and in the same magnitude as *f*CNT, suggesting a significant increase in surface area and/or capacitive species. Electrochemical activation of CP increases its capacitance to (1.4 ± 0.2) ×10^3 μF cm^{-2} and quinone loading to 1.9 ± 0.7 nmol cm^{-2} (Figure 2c). Both values are smaller than those for Act-GC, indicating that electrochemical activation is more effective for GC than CP. Electroactivation of *f*CNT increases capacitance by 7% and quinone loading by 28%. This small increase is likely due to extensive surface oxidation during functionalization, such that there is little potential for further increase. Further optimization of *f*CNT electrochemical activation is under investigation, but so far, Act-*f*CNT is still the most active carbon material in most respects.

dx.doi.org/10.1021/am500087a | ACS Appl. Mater. Interfaces 2014, 6, 6687−6696

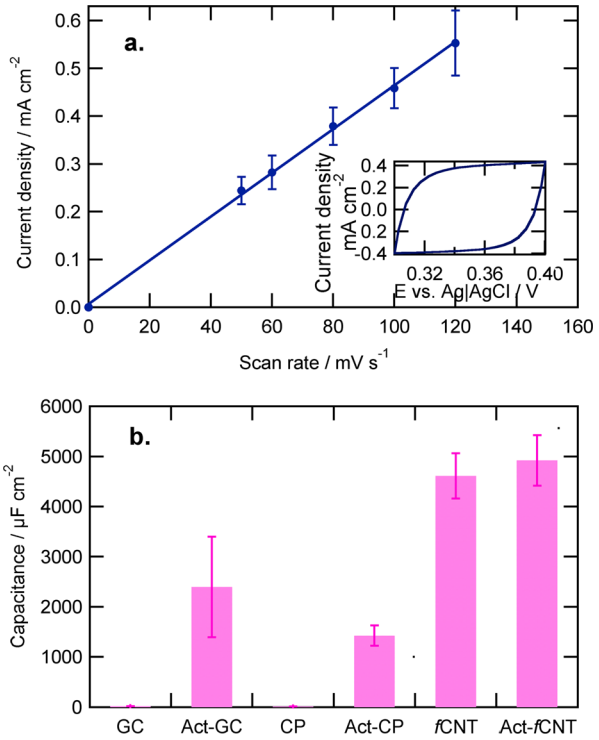

Figure 3. (a) Capacitive current density of *f*CNT as a function of voltammetric scan rate in 0.1 M phosphate buffer, pH 7.4, 30 °C. The slope indicates capacitance. Inset: examples of cyclic voltammograms at 80 mV/s; (b) capacitance of carbon materials.

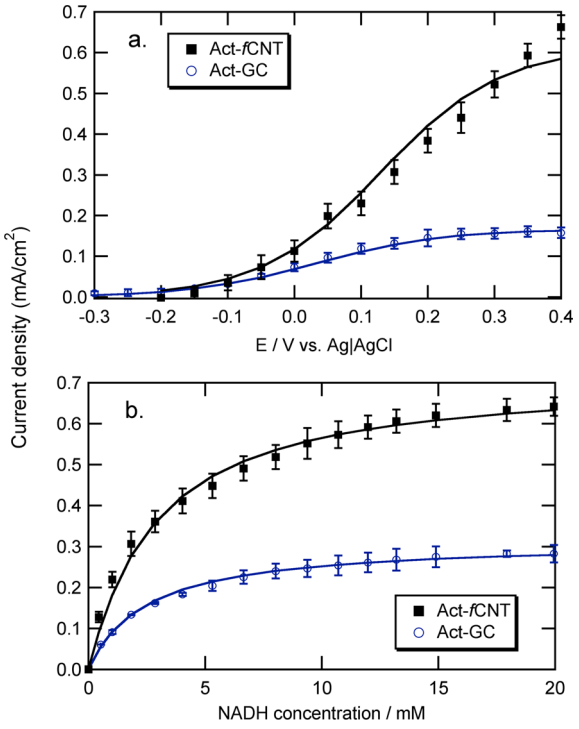

Figure 4. Activity of electrochemically activated GC and *f*CNT for NADH electrocatalysis at 900 rpm in 0.1 M phosphate buffer pH 7.45, 30 °C. The solid lines are mass-transfer-corrected fitting results.[28] (a) Polarization curve in 1 mM NADH; (b) NADH concentration study at 50 mV vs Ag|AgCl.

The catalytic activity of the electroactivated electrodes toward NADH oxidation was studied via polarization and concentration studies. Figure 4 shows polarization curves in fixed NADH concentration (1 mM, Figure 4a) and NADH concentration profiles under fixed applied potential (50 mV vs Ag|AgCl, Figure 4b). Activity toward NADH electrocatalytic oxidation was consistently enhanced by electrochemical activation. This finding is also consistent with literature reported by Čėnas et al.[57] and Prasad et al.[72] In this work, a NADH oxidation current density of 0.28 ± 0.02 mA cm^{-2} was observed for Act-GC at 50 mV vs Ag|AgCl in 20 mM NADH solution (pH 7.45), the same magnitude as that for the Act-*f*CNT electrode (0.64 ± 0.02 mA cm^{-2}) and more than 100-fold higher compared to that for untreated GC (untreated GC data is shown in Supporting Information Figure s1). Electrochemically activated *f*CNT shows a 10% increase in NADH electrocatalysis activity (*f*CNT data is shown in Supporting Information Figure s2), consistent with a marginal increase of capacitance (Figure 3) and quinone loading (Figure 2c).

The enhanced activity of electroactivated electrodes toward NADH oxidation may be attributed to increased active surface area, evidenced by the increase of capacitance, or to NADH electrocatalysis by surface quinone groups (Q):[23,26,73−75]

$$Q + H^+ + NADH \rightleftarrows QH_2 + NAD^+ \quad (3)$$

followed by the recycling of quinone groups on the carbon electrode surface:

$$QH_2 \rightleftarrows Q + 2H^+ + 2e^- \quad (4)$$

Although increased surface area would increase NADH oxidation rate directly, it would not be expected to reduce oxidation overpotential, as quantified by the half-wave potential. However, the introduction of new surface species, such as quinones, can reduce the activation energy, resulting in a reduction in overpotential for NADH oxidation. Table 1 lists half-wave potentials for the materials considered after mass transfer correction.[28] As shown in Table 1 and Figure 4a, Act-GC shows lower half-wave potentials for NADH oxidation than Act-*f*CNT, indicating higher loading of quinones, consistent with higher loading and higher proportion of redox active group as discussed above. Considering these facts, it is likely that the activity of Act-GC is mainly attributed to the quinone groups, while either *f*CNT or Act-*f*CNT serves more as the high surface area material.

Table 1. Half-Wave Potential in NADH Polarization Curves

electrodes	half-wave potential (mV vs Ag|AgCl (4 M KCl))
GC	745 ± 69
Act-GC	27 ± 7
*f*CNT	170 ± 27
Act-*f*CNT	167 ± 25
PMG-*f*CNT	90 ± 23
MG-*f*CNT	24 ± 4

Azine Deposition on Activated Carbon Electrodes. Deposition of MG on the activated GC electrode (Act-GC), CP (Act-CP) and *f*CNT (Act-*f*CNT) were achieved by direct adsorption and the performance of these electrodes was compared to that of electrodes prepared by the electropolymerization method.

Cyclic voltammograms of the resulting MG-Act-GC electrodes are shown in Figure 5a, in which two sets of redox peaks can be observed: the two-step, two-electron redox reaction of

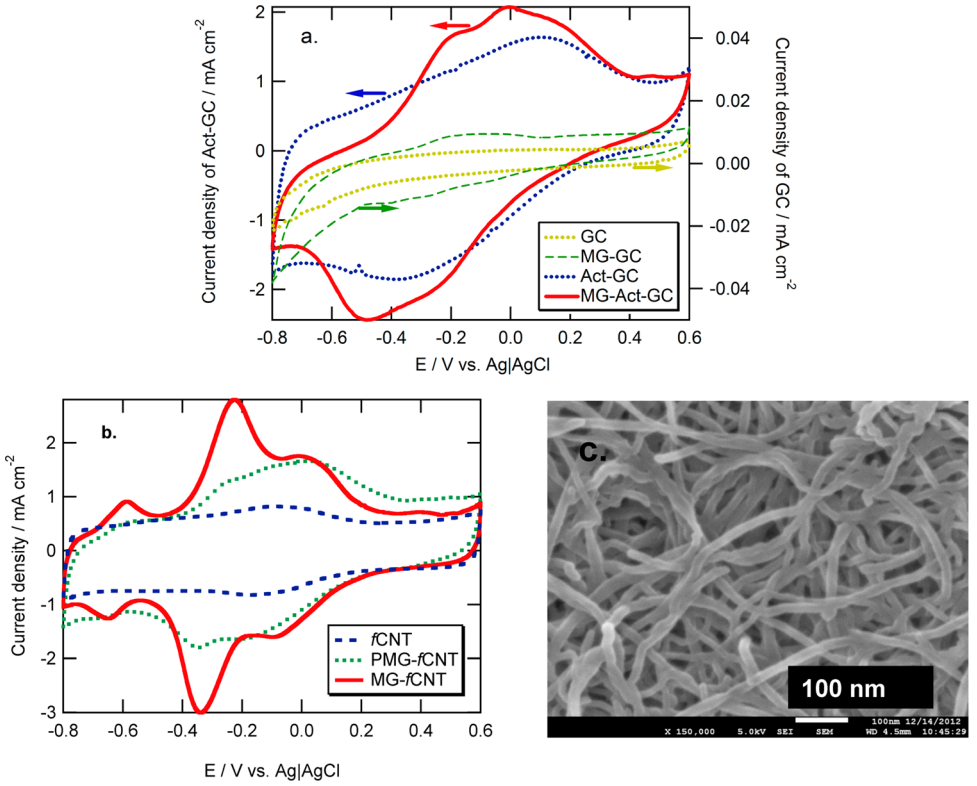

Figure 5. Cyclic voltammograms in 0.1 M phosphate buffer pH 7.45, 30 °C. (a) Adsorbed MG on electrochemically activated GC electrode, compared with activated GC and untreated GC; (b) adsorbed MG on prefunctionalized CNT, compared with electropolymerization on *f*CNT; (c) SEM image of MG-*f*CNT.

MG (at potential −0.5 / −0.2 V, −0.25/0 V) and the redox behavior of quinone groups (at potential−0.3/+0.1 V). The MG redox peak response for MG-Act-GC is 140-fold higher than that for MG-GC, indicating a much stronger adsorption on Act-GC. This could attribute to the stronger electrostatic force between MG and Act-GC, because the oxygen-functionalities on Act-GC make the electrode surface negatively charged, while MG, as a basic dye (pK_a = 9.9), is positively charged in pH 7.4 solution.[76] Other azine dyes were immobilized on Act-GC, including methylene blue (MB) and toluidine blue O (TBO) and found that the most basic dye, MG, shows the strongest adsorption, as shown in Table 2,

Table 2. Azine Adsorption on Act-GC

dye	pK_a[76]	electroactive loading (nmol/cm^2)
methylene green	9.9	40 ± 5
methylene blue	9.3	29 ± 3
toluidine blue O	6.1	34 ± 2

further indicating that electrostatic forces lead to immobilization of azine dyes on Act-GC. Moreover, because TBO is a neutral dye and can also be adsorbed on Act-GC, other adhesive forces must be considered, such as $\pi-\pi$ stacking.[77,78]

In our previous work, we fabricated high-rate, nanostructured NADH oxidizing electrodes by electropolymerizing MG on functionalized CNT (PMG-*f*CNT).[28] In this study, we found that the MG immobilization on *f*CNT could be achieved by adsorption. The resulting electrodes demonstrate improved electroactivity compared to PMG-*f*CNT. The redox behavior of the obtained MG-*f*CNT was characterized via CV and was compared to that of PMG-*f*CNT, as shown in Figure 5b. Peaks in the range −0.5 to +0.2 V vs Ag|AgCl represent the two-step redox reactions of electroactive MG and PMG. PMG redox peaks stay in a slightly positive region than those for MG, consistent with findings on low-surface area electrodes.[65] Integration of the peaks yields electroactive loading of 63 ± 5 nmol cm^{-2} for MG-*f*CNT and 38 ± 4 nmol cm^{-2} for PMG-*f*CNT. This result indicates that MG-*f*CNT possesses more active loading than the previous reported PMG-*f*CNT.

In Figure 5b, it is difficult to discern the broad quinine/hydroquinone peaks on MG-*f*CNT, because they overlap with MG peaks. The redox peak observed with midpoint potential −0.6 V vs Ag|AgCl may be due to impurities in as-received MG, such as methylene blue (MB).[65] MB has a very similar chemical structure to MG and also possesses catalytic activity toward NADH oxidation. However its activity is generally lower than that of MG, as reported by previous researchers.[31,79] Thus, we do not believe the presence of MB explains electrode activity.

The morphology and EDS analysis of the MG-*f*CNT electrode is shown in Figure 5c. From SEM images, no distinct clusters can be observed, suggesting a conformal deposition, similar to PMG-*f*CNT.[28]

The activity of MG-*f*CNT toward NADH electrocatalysis was characterized and is shown in Table 1 and Figure 6 compared to previously reported PMG-*f*CNT-GC. The MG-*f*CNT-GC electrode demonstrates ∼66 mV lower half-wave potential (Table 1) and 1.8-fold current density (Figure 6b) for NADH electrocatalysis, which is corresponding to their CV comparison as discussed previously, demonstrating the improved activity of the MG-*f*CNT interface toward NADH oxidation.

Absorption vs Electropolymerization. As discussed above, the mechanism of adsorption involves electrostatic,

dx.doi.org/10.1021/am500087a | ACS Appl. Mater. Interfaces 2014, 6, 6687−6696

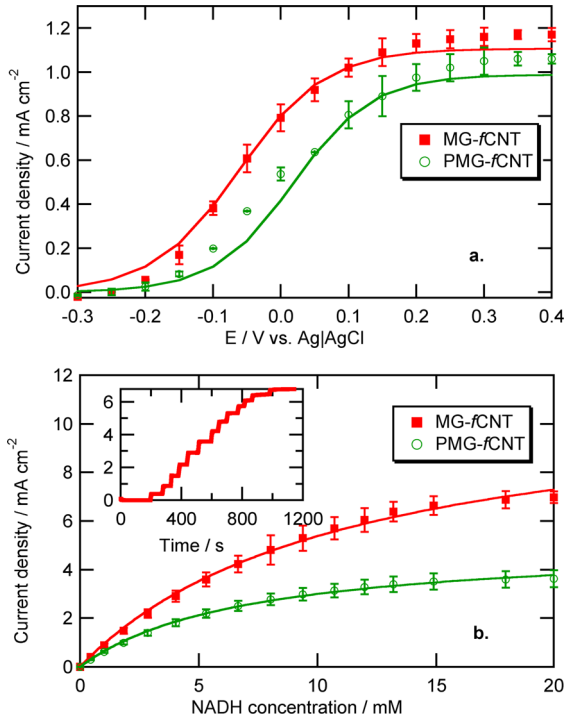

Figure 6. NADH electrocatalysis activity of MG-*f*CNT and PMG-*f*CNT at 900 rpm in 0.1 M phosphate buffer pH 7.45, 30 °C. (a) Polarization curve in 1 mM NADH; (b) NADH concentration study at 50 mV vs Ag|AgCl. Inset: time-dependent curve on MG-*f*CNT.

van der Waals and $\pi-\pi$ stacking forces. The processes of electropolymerization include adsorption of MG, reversible oxidation and reduction of MG and irreversible oxidation of MG to PMG that involves the formation of a cation radical.[28,65,80] The chemical structure and mechanism of formation of PMG is still under investigation. It is believed that PMG has the same redox center as MG (as shown in Figure 7a).[27,65] Hypotheses on PMG formation include "ring-to-ring" coupling, which is analogous to the formation of *N,N,N,N*-tetramethylbenzidine by oxidation of *N,N*-dimethylaniline,[65] and "nitrogen-to-ring" coupling, arising from the observation that destruction of methylene green monomer leads to the demethylation of amino group.[81] Both "ring-to-ring" and "nitrogen-to-ring" types were confirmed via electrospray mass spectrometry as reported by Vilmos et al.[81] The "nitrogen-to-ring" coupling was further confirmed from XPS characterization as reported by Rincón et al.[27] On the basis of these observations, the general proposed chemical structure of PMG is shown in Figure 7b.[27,65,81] Because the coupling sites are far away from the active center of methylene green, the polymerization process is not expected to consume or eliminate redox active sites.

For untreated GC, without the introduction of carbon–oxygen functional groups, the adsorption of MG on GC is relatively weak, and electropolymerization yields a higher electrocatalyst loading and better NADH oxidation activity than MG (Figure 8). Electropolymerization was also used to immobilize PMG on Act-GC. The electropolymerized electrode showed lower electroactive species loading than Act-GC and MG-Act-GC, as shown in Figure 8. Only PMG peaks were found and quinone peaks were not observed. PMG-Act-GC also possessed poorer activity toward NADH electrocatalysis than Act-GC and MG-Act-GC, consistent with its lower loading of redox active groups. It is possible that the irreversible oxidation of MG to PMG during polymerization deactivated some carbon–oxygen functional groups, including quinones, that were introduced in electrochemical activation. This would

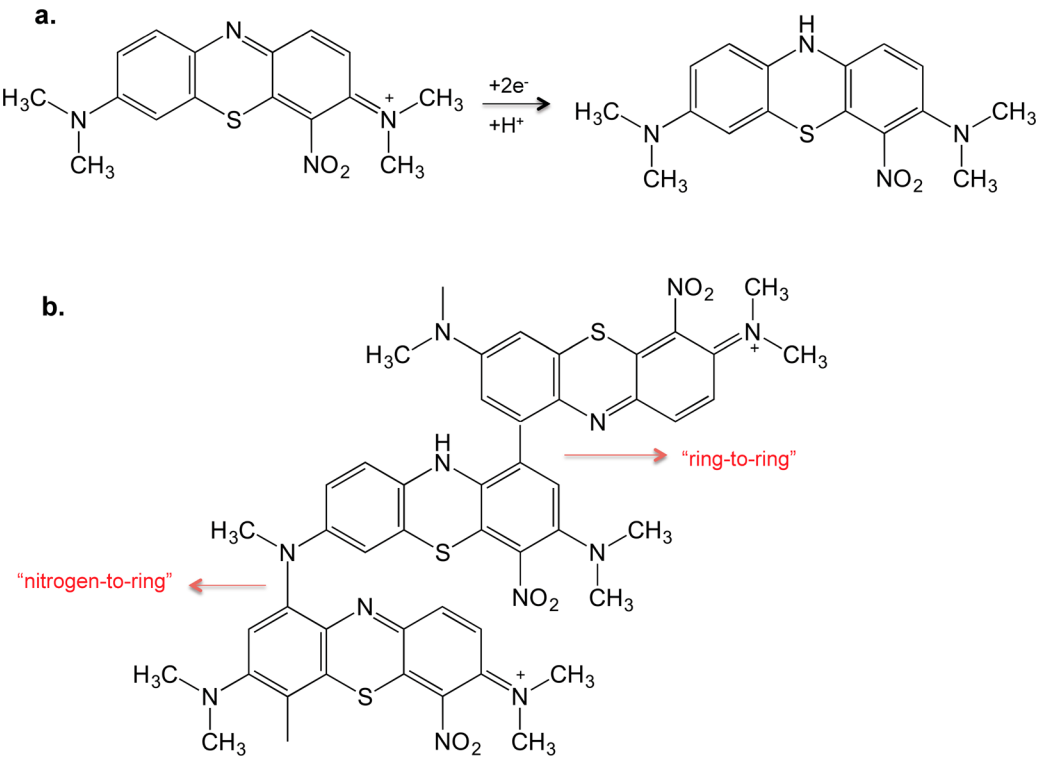

Figure 7. (a) Redox reaction of methylene green; (b) possible structure of poly(methylene green).

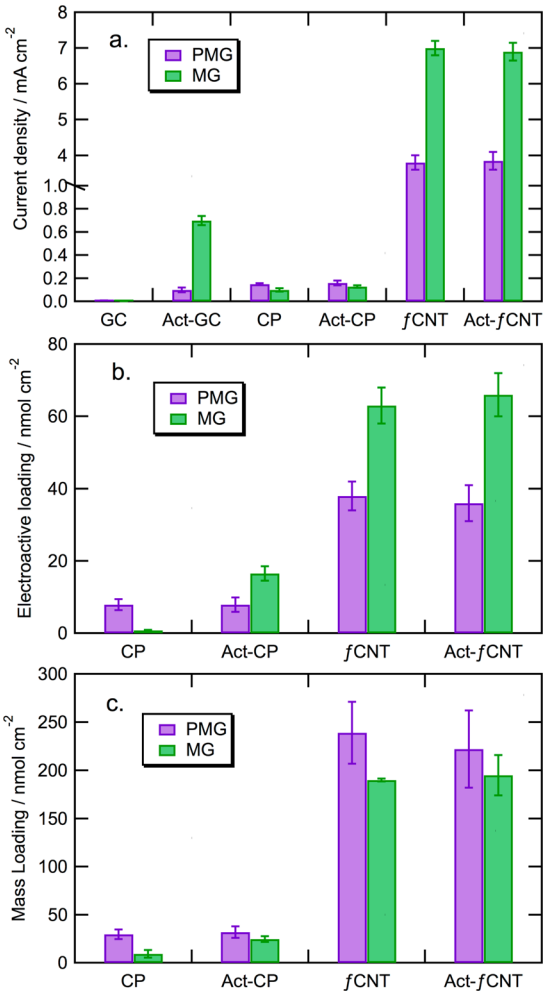

Figure 8. Properties of NADH-oxdizing electrodes. (a) NADH electrocatalysis current recorded at 50 mV vs Ag|AgCl in 20 mM NADH solution, 0.1 M phosphate buffer pH 7.45, 30 °C, 900 rpm; (b) electroactive loading calculated by integration of redox peaks in CV in 0.1 M phosphate buffer pH 7.45, 30 °C, assuming a two-electron redox reaction; (c) MG or PMG loading obtained by EDS based on sulfur content.

lead to lower electroactive loading on PMG-Act-GC, and thus lower activity toward NADH oxidation.

The quantitative comparison of MG and PMG in terms of NADH oxidation activity and electrocatalyst loading is displayed in Figure 8. The MG-Act-GC electrode demonstrates a 0.70 ± 0.04 mA cm^{-2} current density for NADH electro-oxidation (Figure 8a), a 2-fold increase compared to that of Act-GC. Considering the two sets of redox peaks observed in cyclic voltammograms (Figure 5a), electro-oxidation of NADH on MG-Act-GC is likely to be catalyzed by both the quinone groups and MG. After electrochemical activation of *f*CNT, the amount of MG immobilized, either by adsorption (MG) or polymerization (PMG), as well as the resulting catalytic activity remains approximately constant. This could be attributable to a small increase of quinone loading and/or surface area due to *f*CNT electrochemical activation. These results may be improved upon by optimization of *f*CNT electrochemical activation conditions.

Electroactive and mass loading of electrocatalyst are compared for MG and PMG in Figure 8b,c. MG shows higher electroactive loading and lower mass loading than PMG on functionalized carbon materials, suggesting that adsorption provides more efficient utilization of immobilized species than electropolymerization. Taking into account the finding that MG demonstrates higher electrocatalytic activity toward NADH oxidation, adsorption appears to be a more materials-efficient deposition approach than electropolymerization for carbon materials with surface quinoidal functional groups.

Stability. The stability of the modified electrodes was measured by CV between −0.8 and +0.6 vs Ag|AgCl at 900 rpm in pH 7.45 phosphate buffer. Electroactive loadings were obtained by integration of redox peaks in CV, assuming a two-electron redox reaction. MG-Act-GC shows only a 1% decrease in electroactive loading after 100 cycles, comparable with literature data on PMG-GC.[29] As shown in Figure 9, the

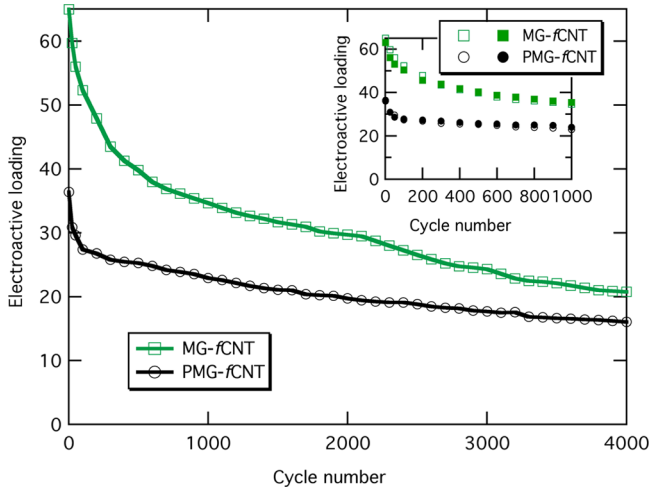

Figure 9. Stability of modified electrodes as measured by cyclic voltammetry (CV) at 900 rpm, 0.1 M phosphate buffer pH 7.45, 30 °C. Electroactive loading was obtained by integration of CV redox peaks, assuming a two-electron redox reaction.

electroactive loading of MG-*f*CNT tends to decrease faster than that of PMG-*f*CNT under CV conditions. Nevertheless, MG-*f*CNT still shows higher loading than PMG-*f*CNT after 4000 continuous cycles, corresponding to its higher initial activity toward NADH oxidation as shown in Table 3.

Table 3. Stability Data

electrodes	initial activity (mA/cm^2)	after 1000 cycles (mA/cm^2)	after 4000 cycles (mA/cm^2)	activity retention after 4000 cycles (%)
MG-ACT-GC	0.70 ± 0.04	0.59 ± 0.03	0.48	69
MG-*f*CNT	7.0 ± 0.2	5.5 ± 0.4	4.9	70
PMG-*f*CNT	3.8 ± 0.2	3.4 ± 0.3	3.1	81

CONCLUSION

Electrochemical activation leads to oxidation of carbon, forming carbon−oxygen functionalities. Some of the functional groups are found to be traces of quinone due to their redox active property and electrocatalytic ability toward NADH oxidation. Other functional groups could lead to an increase of electrochemical capacitance.

Quinone-like functional groups introduced by electrochemical activation appear to directly catalyze NADH oxidation, as well as increase the absorption of azine dyes. Adsorption of MG on electrochemically activated carbon electrodes yields a highly active interface for electro-oxidation of NADH, enabling improved electrochemical regeneration of enzyme cofactors. The stability of adsorbed MG appears to be lower than electropolymerized MG under aggressive cycling conditions, but greater activity is retained after 4000 cycles.

■ ASSOCIATED CONTENT

Supporting Information

Activity of untreated GC for NADH electrocatalysis at 900 rpm, in 0.1 M phosphate buffer pH 7.45, 30 °C and activity of *f*CNT for NADH electrocatalysis at 900 rpm, in 0.1 M phosphate buffer pH 7.45, 30 °C. This material is available free of charge via the Internet at http://pubs.acs.org.

■ AUTHOR INFORMATION

Corresponding Author

*E-mail: scb@msu.edu

Notes

The authors declare no competing financial interest.

■ ACKNOWLEDGMENTS

The authors gratefully acknowledge financial support from the National Science Foundation (Award CBET-0756703).

■ REFERENCES

(1) Voet, D.; Voet, J. G.; Pratt, C. W. *Fundamentals of Biochemistry*, 2nd ed; Wiley: New York, 2002.

(2) Zhou, H.; Zhang, Z.; Yu, P.; Su, L.; Ohsaka, T.; Mao, L. Noncovalent Attachment of NAD^+ Cofactor onto Carbon Nanotubes for Preparation of Integrated Dehydrogenase-Based Electrochemical Biosensors. *Langmuir* **2010**, *26*, 6028−6032.

(3) Moehlenbrock, M. J.; Meredith, M. T.; Minteer, S. D. Bioelectrocatalytic Oxidation of Glucose in CNT Impregnated Hydrogels: Advantages of Synthetic Enzymatic Metabolon Formation. *ACS Catal.* **2011**, *2*, 17−25.

(4) Zhao, X.; Lu, X.; Tze, W. T. Y.; Wang, P. A Single Carbon Fiber Microelectrode with Branching Carbon Nanotubes for Bioelectrochemical Processes. *Biosens. Bioelectron.* **2010**, *25*, 2343−2350.

(5) Eftekhari, A. Glycerol Biosensor Based on Glycerol Dehydrogenase Incorporated into Polyaniline Modified Aluminum Electrode using Hexacyanoferrate as Mediator. *Sens. Actuators, B* **2001**, *80*, 283−289.

(6) Tsai, Y.; Chen, S.; Liaw, H. Immobilization of Lactate Dehydrogenase within Multiwalled Carbon Nanotube-Chitosan Nanocomposite for Application to Lactate Biosensors. *Sens. Actuators, B* **2007**, *125*, 474−481.

(7) Kinoshita, H.; Torimura, M.; Yamamoto, K.; Kano, K.; Ikeda, T. Amperometric Determination of NAD(P)H With Peroxidase-Based H_2O_2-Sensing electrodes and Its Application to Isocitrate Dehydrogenase Activity Assay in Serum. *J. Electroanal. Chem.* **1999**, *478*, 33−39.

(8) Guo, K.; Qian, K.; Zhang, S.; Kong, J. L.; Yu, C. Z.; Liu, B. H. Bio-Electrocatalysis of NADH and Ethanol Based on Graphene Sheets Modified Electrodes. *Talanta* **2011**, *85*, 1174−1179.

(9) Filip, J.; Sefcovicová, J.; Tomcík, P.; Gemeiner, P.; Tkac, J. A Hyaluronic Acid Dispersed Carbon Nanotube Electrode Used for a Mediatorless NADH Sensing and Biosensing. *Talanta* **2011**, *84*, 355−361.

(10) Salimi, A.; Lasghari, S.; Noorbakhash, A. Carbon Nanotubes-Ionic Liquid and Chloropromazine Modified Electrode for Determination of NADH and Fabrication of Ethanol Biosensor. *Electroanalysis* **2010**, *22*, 1707−1716.

(11) Alpat, S.; Telefoncu, A. Development of an Alcohol Dehydrogenase Biosensor for Ethanol Determination with Toluidine Blue O Covalently Attached to a Cellulose Acetate Modified Electrode. *Sensors* **2010**, *10*, 748−764.

(12) Zhou, M.; Zhai, Y. M.; Dong, S. J. Electrochemical Sensing and Biosensing Platform Based on Chemically Reduced Graphene Oxide. *Anal. Chem.* **2009**, *81*, 5603−5613.

(13) Yang, D.; Liu, H. Poly(Brilliant Cresyl Blue)-Carbonnanotube Modified Electrodes for Determination of NADH and Fabrication of Ethanol Dehydrogenase-Based Biosensor. *Biosens. Bioelectron.* **2009**, *25*, 733−738.

(14) Palmore, G. T. R.; Bertschy, H.; Bergens, S. H.; Whitesides, G. M. A Methanol/Dioxygen Biofuel Cell that Uses NAD^+-Dependent Dehydrogenases as Catalysts: Application of an Electro-Enzymatic Method to Regenerate Nicotinamide Adenine Dinucleotide at Low Overpotentials. *J. Electroanal. Chem.* **1998**, *443*, 155−161.

(15) Addo, P.; Arechederra, R.; Minteer, S. Evaluating Enzyme Cascades for Methanol/Air Biofuel Cells Based on NAD^+-Dependent Enzymes. *Electroanalysis* **2010**, *22*, 807−812.

(16) Akers, N. L.; Moore, C. M.; Minteer, S. D. Development of Alcohol/O_2 Biofuel Cells Using Salt-Extracted Tetrabutylammonium Bromide/Nafion Membranes to Immobilize Dehydrogenase Enzymes. *Electrochim. Acta* **2005**, *50*, 2521−2525.

(17) Calabrese Barton, S.; Gallaway, J.; Atanassov, P. Enzymatic Biofuel Cells for Implantable and Microscale Devices. *Chem. Rev.* **2004**, *104*, 4867−4886.

(18) Sokic Lazic, D.; Arechederra, R. L.; Treu, B. L.; Minteer, S. D. Oxidation of Biofuels: Fuel Diversity and Effectiveness of Fuel Oxidation through Multiple Enzyme Cascades. *Electroanalysis* **2010**, *22*, 757−764.

(19) Zhang, Y.; Gao, F.; Zhang, S.; Su, Z.; Ma, G.; Wang, P. Simultaneous Production of 1,3-Dihydroxyacetone and Xylitol from Glycerol and Xylose Using a Nanoparticle-Supported Multi-Enzyme System with in Situ Cofactor Regeneration. *Bioresour. Technol.* **2011**, *102*, 1837−1843.

(20) Zhao, X. Intensified Biocatalysis for Production of Fuel and Chemicals from Lipids. *Ph.D. Thesis*, University of Minnesota: Minnesota, United States, 2010.

(21) Wang, P. In *Bioprocessing for Value-Added Products from Renewable Resources*; Shangtian, Y., Ed; Elsevier: Amsterdam, 2007; Chapter 12, pp 325−350.

(22) El-Zahab, B.; Donnelly, D.; Wang, P. Particle-Tethered NADH for Production of Methanol from CO_2 Catalyzed by Coimmobilized Enzymes. *Biotechnol. Bioeng.* **2008**, *99*, 508−514.

(23) Dicu, D.; Munteanu, F. D.; Popeseu, I. C.; Gorton, L. Indophenol and O-Quinone Derivatives Immobilized on Zirconium Phosphate for NADH Electro-Oxidation. *Anal. Lett.* **2003**, *36*, 1755−1779.

(24) Sato, A.; Kano, K.; Ikeda, T. Diaphorase/Naphthoquinone Derivative-Modified Electrode as an Anode for Diffusion-Controlled Oxidation of NADH in Electrochemical Cells. *Chem. Lett.* **2003**, *32*, 880−881.

(25) Katakis, I.; Dominguez, E. Catalytic Electrooxidation of NADH for Dehydrogenase Amperometric Biosensors. *Mikrochim. Acta* **1997**, *126*, 11−32.

(26) Ma, W.; Li, D. W.; Sutherland, T. C.; Li, Y.; Long, Y. T.; Chen, H. Y. Reversible Redox of NADH and NAD at a Hybrid Lipid Bilayer Membrane Using Ubiquinone. *J. Am. Chem. Soc.* **2011**, *133*, 12366−12369.

(27) Rincón, R.; Artyushkova, K.; Mojica, M.; Germain, M.; Minteer, S.; Atanassov, P. Structure and Electrochemical Properties of Electrocatalysts for NADH Oxidation. *Electroanalysis* **2010**, *22*, 799−806.

(28) Li, H.; Wen, H.; Calabrese Barton, S. NADH Oxidation Catalyzed by Electropolymerized Azines on Carbon Nanotube Modified Electrodes. *Electroanalysis* **2012**, *24*, 398−406.

(29) Dongmei, Z.; Huiqun, F.; Hongyuan, C.; Huangxian, J.; Yun, W. The Electrochemical Polymerization of Methylene Green and its

Electrocatalysis for the Oxidation of NADH. *Anal. Chim. Acta* **1996**, *329*, 41−48.
(30) Karyakin, A. A.; Karyakina, E. E.; Schuhmann, W.; Schmidt, H. L.; Varfolomeyev, S. D. New Amperometric Dehydrogenase Electrodes Based on Electrocatalytic NADH-Oxidation at Poly (Methylene Blue)-Modified Electrodes. *Electroanalysis* **1994**, *6*, 821−829.
(31) Karyakin, A. A.; Karyakina, E. E.; Schuhmann, W.; Schmidt, H. L. Electropolymerized Azines: Part II. In a Search of the Best Electrocatalyst of NADH Oxidation. *Electroanalysis* **1999**, *11*, 553−557.
(32) Bartlett, P. N.; Simon, E.; Toh, C. S. Modified electrodes for NADH oxidation and dehydrogenase-based biosensors. *Bioelectrochemistry* **2002**, *56*, 117−122.
(33) Kim, Y. H.; Yoo, Y. J. Regeneration of the Nicotinamide Cofactor Using a Mediator-Free Electrochemical Method with a Tin Oxide Electrode. *Enzyme Microb. Technol.* **2009**, *44*, 129−134.
(34) Kim, Y. H.; Kim, T.; Ryu, J. H.; Yoo, Y. J. Iron Oxide/Carbon Black (Fe_2O_3/CB) Composite Electrode for the Detection of Reduced Nicotinamide Cofactors Using an Amperometric Method under a Low Overpotential. *Biosens. Bioelectron.* **2010**, *25*, 1160−1165.
(35) Moore, R. R.; Banks, C. E.; Compton, R. G. Basal Plane Pyrolytic Graphite Modified Electrodes: Comparison of Carbon Nanotubes and Graphite Powder as Electrocatalysts. *Anal. Chem.* **2004**, *76*, 2677−2682.
(36) Zhang, L.; Li, Y.; Li, D. W.; Karpuzov, D.; Long, Y. T. Electrocatalytic Oxidation of NADH on Graphene Oxide and Reduced Graphene Oxide Modified Screen-Printed Electrode. *Int. J. Electrochem. Sci.* **2011**, *6*, 819−829.
(37) Wooten, M.; Gorski, W. Facilitation of NADH Electro-Oxidation at Treated Carbon Nanotubes. *Anal. Chem.* **2010**, *82*, 1299−1304.
(38) Narváez Villarrubia, C. W.; Rincón, R. A.; Radhakrishnan, V. K.; Davis, V.; Atanassov, P. Methylene Green Electrodeposited on SWNTs-Based "Bucky" Papers for NADH and L-Malate Oxidation. *ACS Appl. Mater. Interfaces* **2011**, *3*, 2402−2409.
(39) Li, H.; Worley, K. E.; Calabrese Barton, S. Quantitative Analysis of Bioactive NAD Regenerated by NADH Electro-oxidation. *ACS Catal.* **2012**, *2*, 2572−2576.
(40) McCreery, R. L. Advanced Carbon Electrode Materials for Molecular Electrochemistry. *Chem. Rev.* **2008**, *108*, 2646−2687.
(41) Eisenberg, E. J.; Cundy, K. C. Amperometric High-Performance Liquid-Chromatographic Detection of NADH at a Base-Activated Glassy-Carbon Electrode. *Anal. Chem.* **1991**, *63*, 845−847.
(42) Liu, X. Q.; Li, B. H.; Li, C. Y. Sensitive Determination of Dihydronicotinamide Adenine Dinucleotide and Ethanol with a Nano-Porous Carbon Electrode. *J. Serb. Chem. Soc.* **2011**, *76*, 113−123.
(43) Hung Tzang, C.; Yuan, R.; Yang, M. Voltammetric Biosensors for the Determination of Formate and Glucose-6-Phosphate Based on the Measurement of Dehydrogenase-Generated NADH and NADPH. *Biosens. Bioelectron.* **2001**, *16*, 211−219.
(44) Zare, H. R.; Samimi, R.; Mazloum Ardakani, M. A Comparison of the Electrochemical Behavior of Rutin at an Inactivated, Activated, and Multi Wall Carbon Nanotubes Modified Glassy Carbon Electrode. *Int. J. Electrochem. Sci.* **2009**, *4*, 730−739.
(45) Golabi, S. M.; Irannejad, L. Preparation and Electrochemical Study of Fisetin Modified Glassy Carbon Electrode. Application to the Determination of NADH and Ascorbic Acid. *Electroanalysis* **2005**, *17*, 985−996.
(46) Zare, H. R.; Eslami, M.; Namazian, M. Electrochemical Behavior of O-Chloranil in Aqueous Solution at an Activated Glassy Carbon Electrode. *Electrochim. Acta* **2011**, *56*, 2160−2164.
(47) Ahammad, A. J. S.; Sarker, S.; Rahman, M. A.; Lee, J. J. Simultaneous Determination of Hydroquinone and Catechol at an Activated Glassy Carbon Electrode. *Electroanalysis* **2010**, *22*, 694−700.
(48) Hance, G. W.; Kuwana, T. Effect of Glassy Carbon Pretreatment on Background Double-Layer Capacitance and Adsorption of Neutral Organic Molecules. *Anal. Chem.* **1987**, *59*, 131−134.
(49) Allred, C. D.; McCreery, R. L. Adsorption of Catechols on Fractured Glassy Carbon Electrode Surfaces. *Anal. Chem.* **1992**, *64*, 444−448.
(50) Zhang, H.; Coury, L. A. Effects of High-Intensity Ultrasound on Glassy Carbon Electrodes. *Anal. Chem.* **1993**, *65*, 1552−1558.
(51) Rice, R. J.; Pontikos, N. M.; McCreery, R. L. Quantitative Correlations of Heterogeneous Electron-Transfer Kinetics with Surface Properties of Glassy Carbon Electrodes. *J. Am. Chem. Soc.* **1990**, *112*, 4617−4622.
(52) Epstein, B. D.; Dallemol, E.; Mattson, J. S. Electrochemical Investigations of Surface Functional Groups on Isotropic Pyrolytic Carbon. *Carbon* **1971**, *9*, 609−615.
(53) Pontikos, N. M.; McCreery, R. L. Microstructural and Morphological Changes Induced in Glassy Carbon Electrodes by Laser Irradiation. *J. Electroanal. Chem.* **1992**, *324*, 229−242.
(54) Tominaga, M.; Sakamoto, S.; Yamaguchi, H. Jungle-Gym Structured Films of Single-Walled Carbon Nanotubes on a Gold Surface: Oxidative Treatment and Electrochemical Properties. *J. Phys. Chem. C* **2012**, *116*, 9498−9506.
(55) Van der Linden, W. E.; Dieker, J. W. Glassy Carbon as Electrode Material in Electroanalytical Chemistry. *Anal. Chim. Acta* **1980**, *119*, 1−24.
(56) Laser, D.; Ariel, M. The Anodic Behavior of Glassy Carbon in Acid Solution: A Spectroelectrochemical Study. *J. Electroanal. Chem. Interfacial Electrochem.* **1974**, *52*, 291−303.
(57) Cenas, N.; Rozgaite, J.; Pocius, A.; Kulys, J. Electrocatalytic Oxidation of NADH and Ascorbic-Acid on Electrochemically Pretreated Glassy-Carbon Electrodes. *J. Electroanal. Chem.* **1983**, *154*, 121−128.
(58) Calabrese Barton, S.; Sun, Y.; Chandra, B.; White, S.; Hone, J. Mediated Enzyme Electrodes with Combined Micro- and Nanoscale Supports. *Electrochem. Solid-State Lett.* **2007**, *10*, B96−B100.
(59) Kinoshita, K. *Carbon: Electrochemical and Physicochemical Properties*, 1st ed.; Wiley: New York, 1988.
(60) Chakraborty, S.; Raj, C. R. Mediated Electrocatalytic Oxidation of Bioanalytes and Biosensing of Glutamate using Functionalized Multiwall Carbon Nanotubes-Biopolymer Nanocomposite. *J. Electroanal. Chem.* **2007**, *609*, 155−162.
(61) Chen, J.; Bao, J.; Cai, C.; Lu, T. Electrocatalytic Oxidation of NADH at an Ordered Carbon Nanotubes Modified Glassy Carbon Electrode. *Anal. Chim. Acta* **2004**, *516*, 29−34.
(62) Gong, K.; Chakrabarti, S.; Dai, L. Electrochemistry at Carbon Nanotube Electrodes: Is the Nanotube Tip More Active Than the Sidewall? *Angew. Chem., Int. Ed.* **2008**, *47*, 5446−5450.
(63) Musameh, M.; Lawrence, N. S.; Wang, J. Electrochemical Activation of Carbon Nanotubes. *Electrochem. Commun.* **2005**, *7*, 14−18.
(64) Wen, H.; Nallathambi, V.; Chakraborty, D.; Calabrese Barton, S. Carbon Fiber Microelectrodes Modified with Carbon Nanotubes as a New Support for Immobilization of Glucose Oxidase. *Microchim. Acta* **2012**, *175*, 283−289.
(65) Karyakin, A. A.; Karyakina, E. E.; Schmidt, H. L. Electropolymerized Azines: A New Group of Electroactive Polymers. *Electroanalysis* **1999**, *11*, 149−155.
(66) Flegler, S. L.; Heckman, J. W.; Klomparens, K. L. *Scanning and Transmission Electron Microscopy: an Introduction*; Oxford University Press: Oxford, U.K., 1993.
(67) Jenkins, G. M.; Kawamura, K. Structure of Glassy Carbon. *Nature* **1971**, *231*, 175−176.
(68) Dekanski, A.; Stevanović, J.; Stevanović, R.; Nikolić, B. Ž.; Jovanović, V. M. Glassy Carbon Electrodes: I. Characterization and Electrochemical Activation. *Carbon* **2001**, *39*, 1195−1205.
(69) Figueiredo, J. L.; Pereira, M. F. R.; Freitas, M. M. A.; Órfão, J. J. M. Modification of the Surface Chemistry of Activated Carbons. *Carbon* **1999**, *37*, 1379−1389.
(70) Kepley, L. J.; Bard, A. J. Ellipsometric, Electrochemical, and Elemental Characterization of the Surface Phase Produced on Glassy-Carbon Electrodes by Electrochemical Activation. *Anal. Chem.* **1988**, *60*, 1459−1467.

(71) Dewar, M. J. S.; Trinajstic, N. Ground States of Conjugated Molecules - XIV: Redox Potentials of Quinones. *Tetrahedron* **1969**, *25*, 4529−4534.
(72) Prasad, K. S.; Chen, J. C.; Ay, C.; Zen, J. M. Mediatorless Catalytic Oxidation of NADH at a Disposable Electrochemical Sensor. *Sens. Actuators, B* **2007**, *123*, 715−719.
(73) Wang, J.; Peng, T. Enhanced Stability of Glassy Carbon Detectors Following a Simple Electrochemical Pretreatment. *Anal. Chem.* **1986**, *58*, 1787−1790.
(74) Ma, W.; Long, Y. Quinone/Hydroquinone-Functionalized Biointerfaces for Biological Applications from the Macro- to Nano-Scale. *Chem. Soc. Rev.* **2014**, *43*, 30−41.
(75) Ma, W.; Ying, Y. L.; Qin, L. X.; Gu, Z.; Zhou, H.; Li, D. W.; Sutherland, T. C.; Chen, H. Y.; Long, Y. T. Investigating Electron-Transfer Processes Using a Biomimetic Hybrid Bilayer Membrane System. *Nat. Protoc.* **2013**, *8*, 439−450.
(76) Woislawski, S. The Spectrophotometric Determination of Ionization Constants of Basic Dyes. *J. Am. Chem. Soc.* **1953**, *75*, 5201−5203.
(77) Pereira, M. F. R.; Soares, S. F.; Órfão, J. J. M.; Figueiredo, J. L. Adsorption of Dyes on Activated Carbons: Influence of Surface Chemical Groups. *Carbon* **2003**, *41*, 811−821.
(78) Faria, P. C. C.; Órfão, J. J. M.; Pereira, M. F. R. Adsorption of Anionic and Cationic Dyes on Activated Carbons with Different Surface Chemistries. *Water Res.* **2004**, *38*, 2043−2052.
(79) Blackwell, A. E.; Moehlenbrock, M. J.; Worsham, J. R.; Minteer, S. D. Comparison of electropolymerized thiazine dyes as an electrocatalyst in enzymatic biofuel cells and self powered sensors. *J. Nanosci. Nanotechnol.* **2009**, *9*, 1714−1721.
(80) Karyakin, A. A.; Strakhova, A. K.; Karyakina, E. E.; Varfolomeyev, S. D.; Yatsimirsky, A. K. The electrochemical polymerization of methylene blue and bioelectrochemical activity of the resulting film. *Bioelectrochem. Bioenerg.* **1993**, *32*, 35−43.
(81) Vilmos, K.; Gary, J. V. B. Electropolymerization of Methylene Blue Investigated Using On-Line Electrochemistry/Electrospray Mass Spectrometry. *Electroanalysis* **2001**, *13*, 1425−1430.